Superconducting mesoscopic square loop

V. M. Fomin,* V. R. Misko,† and J. T. Devreese‡
Theoretische Fysica van de Vaste Stof, Universiteit Antwerpen (U.I.A.), Universiteitsplein 1, B-2610 Antwerpen, Belgium

V. V. Moshchalkov
Laboratorium voor Vaste Stoffysica en Magnetisme, Katholieke Universiteit Leuven, Celestijnenlaan 200 D, B-3001 Leuven, Belgium
(Received 9 September 1997; revised manuscript received 6 July 1998)

For a superconducting mesoscopic square loop, the superconducting state is described and the phase boundaries are analyzed on the basis of a self-consistent solution of the Ginzburg-Landau equations. There exists a qualitative difference in the nucleation of the superconducting state in a square and a circular mesoscopic loop. Due to the interplay of different kinds of symmetry, of the square loop and of the magnetic field, the order-parameter distribution is inhomogeneous in the loop. After clarification of the thermodynamical stability of the superconducting states, we turn to the analysis of the equilibrium states which can be realized in experiment. The problem of the *H-T* superconducting phase boundary is discussed in detail. The calculated phase boundaries are in good agreement with the experimental data obtained for the Al mesoscopic superconducting square loops. [S0163-1829(98)06741-1]

I. INTRODUCTION

Three well-known experiments on persistent currents in metallic[1,2] and semiconducting[3] mesoscopic rings have stimulated intensive theoretical research of quantization and confinement effects in nanosize metallic and semiconducting structures. Recently, these effects have also been studied in mesoscopic superconducting structures. The experiments[4,5] carried out on superconducting mesoscopic aluminum loops with sizes smaller than the temperature-dependent coherence length $\xi(T)$ and the penetration depth $\lambda(T)$ reveal the influence of the sample topology on the superconducting critical parameters, such as critical temperature T_c as a function of magnetic field H. Also the resistive transition anomalies have been observed in multiprobe aluminum nanostructures with a linewidth less than 100 nm.[6,7] Quite recently, the susceptibility of a single mesoscopic aluminum ring was experimentally studied with an integrated superconducting quantum interference device at temperatures near the superconducting critical temperature.[8] These experiments have focussed on the problem of the $T_c(H)$ phase boundary in the mesoscopic superconductor structures of different topology, which is the central point of the present paper.

In a mesoscopic *square* loop, the Little-Parks-type oscillating *H-T* phase boundary has been detected; it is related to the effect of the fluxoid quantization in the loop.[4] To interpret these oscillations, the authors of Ref. 4 applied the Tinkham formula[9] which describes the superconducting transition in a perpendicular magnetic field for a *circular* loop with emphasis on the consequences of flux quantization. After analysis by Tinkham, there has been a long-standing interest in the superconducting properties of samples possessing *cylindrical symmetry*. For example, the oscillating dependence of the critical magnetic vortex-nucleation field was investigated for a *cylinder* and a *cylindrical pore* in a superconducting matrix (see, e.g., Ref. 10), in particular, when their radius is of the order of the coherence length $\xi(T)$.[11] The analysis by de Gennes of the onset of superconductivity in a thin ring carrying a lateral arm[12] was of importance for the explanation of the effect of topology on the $T_c(H)$ dependence. Recently, nucleation and evolution of the order parameter and the critical temperature were analyzed near a circular hole.[13]

Although the observed $T_c(H)$ oscillations can be interpreted in the above-described way by choosing some effective radii of cylinders, nevertheless the experimental investigation of mesoscopic superconducting structures of realistic shape (e.g., square loops) requires a more adequate theoretical description. To the best of our knowledge, there have been no theoretical reports on the superconducting properties of *square-shaped loops*, relevant to the available experiments.

In our theoretical analysis we rely upon the Ginzburg-Landau (GL) equations for the order parameter ψ and the vector potential $\mathbf{A}$ of a magnetic field $\mathbf{H}=\mathrm{rot}\mathbf{A}$,[14–16]

$$\frac{1}{2m}\left(-i\hbar\nabla-\frac{2e}{c}\mathbf{A}\right)^2\psi+a\psi+b|\psi|^2\psi=0, \tag{1}$$

$$\Delta\mathbf{A}=\frac{4\pi ie\hbar}{mc}(\psi^*\nabla\psi-\psi\nabla\psi^*)+\frac{16\pi e^2}{mc^2}\mathbf{A}|\psi|^2. \tag{2}$$

Here a and b are the GL parameters. We use the following boundary condition:

$$\mathbf{n}\cdot\left(-i\hbar\nabla\psi-\frac{2e}{c}\mathbf{A}\psi\right)\Big|_{boundary}=0, \tag{3}$$

where $\mathbf{n}$ is the unit vector normal to the boundary. It is important to mention here, that the geometry of a real superconducting structure enters the problem via the boundary condition (3).

The paper is organized as follows. The discussion of the boundary problem for a loop is forwarded in Sec. II by the analysis of the phase boundary of a superconductor filling a corner in terms of a variational model based on the linearized

GL theory. This simple approach allows one to elaborate an insight into the edge effects in superconducting square loops having such corners.

The main topic of the paper is a self-consistent solution of the GL equations for a mesoscopic square superconducting loop. The basic equations with the appropriate boundary conditions are derived in Sec. III. Section IV is devoted to the discussion of the obtained solutions. The distributions of the magnetic field $H(x,y)$, of the squared amplitude $\psi_a^2(x,y)$, and of the phase $\phi(x,y)$ of the order parameter $\psi=\psi_a\exp(i\phi)$ are presented for the cases when an enclosed fluxoid contains a different number L of magnetic flux quanta Φ_0. It is shown how the found distributions depend on the temperature and on the applied magnetic field and how they change for various fixed orbital momenta L. The influence of the length of leads on distributions of the magnetic field and the order parameter is revealed. The differences in ψ_a at midpoints of the adjacent sides of the loop are discussed in relation to the experimental measurements of the $T_c(H)$. After clarification of the thermodynamical stability of the superconducting states, we turn to the equilibrium states which can be realized in experiment. In Sec. V, the problem of the definition of the $T_c(H)$ phase boundary for a square loop is analyzed. It is demonstrated that the theoretical results fit quite well with available experimental data.[4,5]

II. THE NUCLEATION OF THE SUPERCONDUCTING STATE IN THE WEDGE

Before analyzing the superconducting state in a square loop, we consider first the problem of a ''superconducting corner,'' i.e., the nucleation of superconductivity in a wedge-like sample with magnetic field applied parallel to the wedge's edge. A superconductor, which fills a corner with the central angle α $(0<\alpha<2\pi)$ and is restricted by the two planes $\varphi=0$, $\varphi=\alpha$, is considered in the presence of a uniform magnetic field $\mathbf{H}=H\mathbf{e}_z$. With the origin of coordinates chosen at the edge of the corner, it is convenient to use the vector potential of the magnetic field in the symmetrical gauge:

$$\mathbf{A}=A_x\mathbf{e}_x+A_y\mathbf{e}_y,\quad A_y=\tfrac{1}{2}Hx,\quad A_x=-\tfrac{1}{2}Hy, \tag{4}$$

or in cylindrical coordinates,

$$\mathbf{A}=A_\varphi(\rho)\mathbf{e}_\varphi,\quad A_\varphi(\rho)=\tfrac{1}{2}H\rho. \tag{5}$$

The linearized GL equation (1) (see Refs. 14–16)

$$\frac{1}{2m}\left(-i\hbar\nabla-\frac{2e}{c}\mathbf{A}\right)^2\Psi+a\Psi=0 \tag{6}$$

in cylindrical coordinates takes on the form

$$-\frac{\hbar^2}{2m}\left\{\frac{1}{\rho}\frac{\partial}{\partial\rho}\left(\rho\frac{\partial\Psi}{\partial\rho}\right)+\left[\frac{1}{\rho}\frac{\partial}{\partial\varphi}+\frac{2e}{ic\hbar}\mathbf{A}(\rho)\right]^2\Psi\right\}=-a\Psi. \tag{7}$$

Inserting here Eq. (5) and the coherence length $\xi=\hbar/(\sqrt{2m|a|})$, we obtain

$$-\left\{\frac{1}{\rho}\frac{\partial}{\partial\rho}\left(\rho\frac{\partial\Psi}{\partial\rho}\right)+\left[\frac{1}{\rho}\frac{\partial}{\partial\varphi}+\frac{eH}{ic\hbar}\rho\right]^2\Psi\right\}=\frac{1}{\xi^2}\Psi. \tag{8}$$

In terms of the dimensionless variable $\rho'=\rho\sqrt{eH/c\hbar}$ and the coherence length $\xi'=\xi\sqrt{eH/c\hbar}$, this equation can be written as

$$-\left\{\frac{1}{\rho'}\frac{\partial}{\partial\rho'}\left(\rho'\frac{\partial\Psi}{\partial\rho'}\right)+\frac{1}{\rho'^2}\left[\frac{\partial}{\partial\varphi}-i\rho'^2\right]^2\Psi\right\}=\frac{1}{\xi'^2}\Psi. \tag{9}$$

It is important to mention the relation with the second critical field H_{c2}

$$\frac{1}{\xi'^2}=\frac{2H_{c2}}{H}, \tag{10}$$

which can be used to define the critical magnetic field in a corner as

$$H_{crit}=\max H=\frac{2H_{c2}}{\min(1/\xi'^2)}. \tag{11}$$

This field is therefore determined by the minimal value of the inverse squared dimensionless coherence length ξ'^2.

Unit vectors normal to the planes $\varphi=0$ and $\varphi=\alpha$ forming a wedge are $\mathbf{e}_\varphi$ and $-\mathbf{e}_\varphi$, respectively. Hence, the boundary conditions (3) for the order parameter are

$$\left(-i\frac{1}{\rho}\frac{\partial\Psi}{\partial\varphi}-\frac{eH}{c\hbar}\rho\Psi\right)\Bigg|_{\varphi=0,\alpha}=0. \tag{12}$$

After introducing the dimensionless radial variable ρ', Eq. (12) turns to

$$\left(i\frac{\partial\Psi}{\partial\varphi}+\rho'^2\Psi\right)\Bigg|_{\varphi=0,\alpha}=0. \tag{13}$$

Henceforth, the prime in the denotation ρ' will be omitted for simplicity.

The solution of Eq. (9) with boundary conditions (13) will be sought in the form

$$\Psi(\rho,\varphi)=\exp\left[\frac{i\rho^2\sin(2\pi n\varphi/\alpha)}{2\pi n/\alpha}\right]f_n(\rho,\varphi),$$

$$n=0,1,2,\ldots. \tag{14}$$

In order to satisfy the boundary conditions (13), we choose vanishing derivatives of the new function $f_n(\rho,\varphi)$ with respect to the angle at the boundaries:

$$\frac{\partial f_n}{\partial\varphi}\Bigg|_{\varphi=0,\alpha}=0. \tag{15}$$

Indeed,

$$\frac{\partial\Psi(\rho,\varphi)}{\partial\varphi}=i\rho^2\cos(2\pi n\varphi/\alpha)\Psi(\rho,\varphi)$$

$$+\exp\left[\frac{i\rho^2\sin(2\pi n\varphi/\alpha)}{2\pi n/\alpha}\right]\frac{\partial f_n(\rho,\varphi)}{\partial\varphi}, \tag{16}$$

wherefrom Eqs. (13) follow straightforwardly.

The equation for the new function $f_n(\rho,\varphi)$ reads

$$\hat{O}f_n(\rho,\varphi)=\frac{1}{\xi'^2}f_n(\rho,\varphi), \tag{17}$$

$$\begin{aligned}\hat{O}f_n(\rho,\varphi)\equiv i\Bigg\{&\sin(2\pi n\varphi/\alpha)\left[\left(\frac{2\pi n}{\alpha}-\frac{4}{(2\pi n/\alpha)}\right)f_n(\rho,\varphi)\right.\\&\left.-4\rho\frac{\partial f_n(\rho,\varphi)}{\partial\rho}\right]+2\sin^2(\pi n\varphi/\alpha)\frac{\partial f_n(\rho,\varphi)}{\partial\varphi}\Bigg\}\\&+4\rho^2\left[\left(\frac{\sin(2\pi n\varphi/\alpha)}{2\pi n/\alpha}\right)^2+\sin^4(\pi n\varphi/\alpha)\right]\\&\times f_n(\rho,\varphi)-\frac{1}{\rho}\frac{\partial f_n(\rho,\varphi)}{\partial\rho}-\frac{\partial^2 f_n(\rho,\varphi)}{\partial\rho^2}\\&-\frac{1}{\rho^2}\frac{\partial^2 f_n(\rho,\varphi)}{\partial\varphi^2}.\end{aligned}$$

In order to solve this differential equation, we apply a variational method, which is a generalization of the variational approach, proposed by Kittel and used by de Gennes for a semi-infinite semiconductor plane,[16] to a wedge with an arbitrary value of the angle α. Namely, for a given trial function $f_n(\rho,\varphi)$, both parts of Eq. (17) are multiplied by $f_n^*(\rho,\varphi)$. Upon integration over the area of the corner, the following expression for $1/\xi'^2$ results:

$$\frac{1}{\xi'^2}=\frac{\int_{\text{corner}} f_n^*(\rho,\varphi)\hat{O}f_n(\rho,\varphi)\rho d\rho d\varphi}{\int_{\text{corner}}|f_n(\rho,\varphi)|^2\rho d\rho d\varphi}. \tag{18}$$

Two types of the trial functions are further used (for certainty, $n=1$ is taken henceforth)

$$f(\rho,\varphi)=\exp\left[ik\cos\left(\frac{\pi\varphi}{\alpha}\right)\right]\exp\left[-r\rho\left(1-\frac{\alpha}{\pi}\cos^2\frac{\pi\varphi}{\alpha}\right)\right], \tag{19}$$

$$f_\mu(\rho,\varphi)=\rho^{(\mu-1)/2}\exp\left[ik\cos\left(\frac{\pi\varphi}{\alpha}\right)\right]\exp\left[-r\rho\left(\sin^2\frac{\pi\varphi}{\alpha}\right)\right]. \tag{20}$$

We would like to emphasize that for a semi-infinite semiconductor plane (i.e., for $\alpha=\pi$) both trial functions (19) and (20) turn to the function, proposed by Kittel (see Ref. 16). After substituting these functions into the right-hand side of Eq. (18), the resulting expression for $1/\xi'^2$ is minimized with respect to the variational parameters k,r.

The resulting distributions of the order parameter in the corner are shown in Fig. 1 for three different values of the angle $\alpha=0.05\pi$, 0.5π, 1.5π. For $\alpha<\pi$ and $\alpha>\pi$, the minimum of $1/\xi'^2$ is provided by the trial functions of the type (19) and (20), correspondingly. The obtained solutions clearly indicate that for $0<\alpha<\pi$ there appears a *maximum* of the order parameter at the edge of the corner. This general feature of the model implies that the nucleation of the superconducting phase in the corner is facilitated in the vicinity of the edge, i.e., superconductivity in the corners sustains substantially higher applied fields. Extrapolating these results to a square loop, we can already anticipate a stronger superconductivity of the corners.

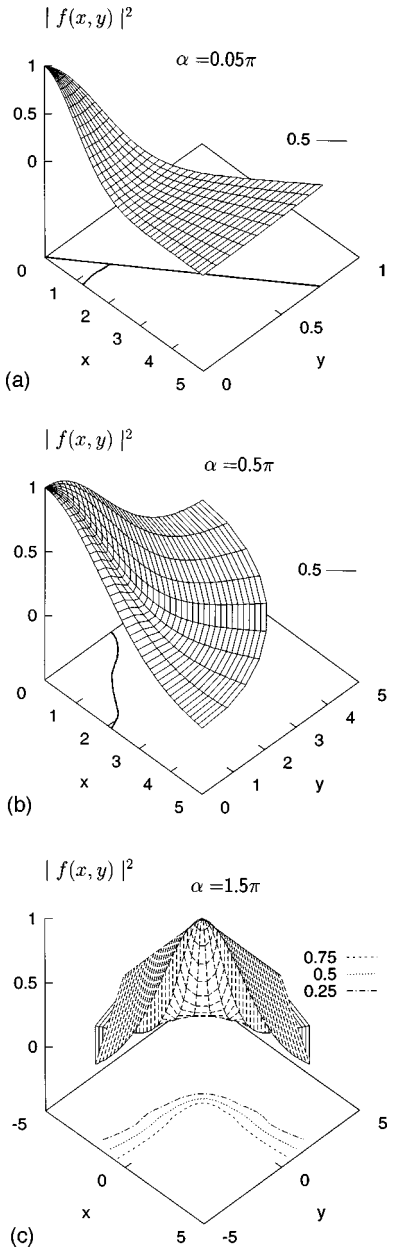

FIG. 1. Distributions of the order parameter $|f(\rho,\varphi)|^2$ in the corner with the central angle $\alpha=0.05\pi$ (a), 0.5π (b), 1.5π (c). Calculations were performed using Eq. (19) for the cases (a), (b) and Eq. (20) with $\mu=1$ for the case (c), respectively.

III. THE BOUNDARY PROBLEM FOR A MESOSCOPIC SQUARE LOOP

In this section, we consider a mesoscopic structure of a type-II superconductor with the shape of a square loop with leads (see Fig. 2). The leads are made from the same material as the loop and are supposed to have the same width as the loop itself. This corresponds to the shape of the real structure which has been studied in the experiments reported in Ref. 4. We take the following sizes of the loop: the width $d=150$ nm, the outer side $Q_e=1000$ nm (the side of the

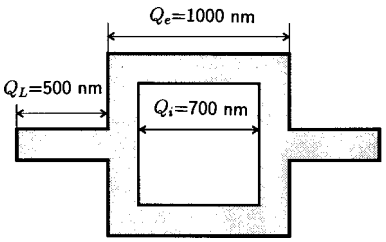

FIG. 2. Scheme of a mesoscopic superconducting square loop with leads.

opening, therefore, is $Q_i = 700$ nm), and the length of the leads is $Q_l = 500$ nm (the case when the length of the leads changes will be specially discussed).

In order to adapt our model to the experimental conditions, we used in the calculations the values of the Ginzburg-Landau parameters taken from the relevant experimental works (Refs. 4 and 5). These values differ essentially from the corresponding values for bulk Al, e.g., the Ginzburg-Landau parameter κ has the value of 0.03 (Ref. 17) in pure bulk aluminum, but its value in the mesoscopic loop under consideration is close to unity. As it follows from Refs. 4 and 5, $\xi_0 = 100$ nm, $\lambda_0 = 91$ nm, that gives $\kappa = 0.91$. Hence, the characteristics of the structure under consideration are introduced in the equations through the relevant values of the Ginzburg-Landau parameters.

The magnetic field H_0 is applied in the z direction, i.e., perpendicular to the sample which lies in the xy plane. In our calculations, we will consider all the relevant physical quantities, namely, the magnetic field in the structure H, the phase ϕ, and the squared amplitude ψ_a^2 of the order parameter, as functions of x and y whereas the z dependence will be neglected. This simplification does not influence substantially the results as far as the specific features of the magnetic field and the order-parameter distributions inside the loop are due to the complex shape of the cross section of the superconducting structure in the xy plane. It is clear that our assumption is adequate for very thin plates or for samples extended in the z direction, as long as the magnetic field is uniform in this direction.

For the geometry of the problem under consideration in the case of a uniform magnetic field, the suitable form of the symmetrical gauge for the vector potential $\mathbf{A}$ is

$$\mathbf{A} = \tfrac{1}{2}[\mathbf{H} \times \mathbf{r}], \tag{21}$$

where $\mathbf{H} = H\mathbf{e}_z$ is the magnetic field strength, and $\mathbf{r} = x\mathbf{e}_x + y\mathbf{e}_y$. In the case of a nonuniform magnetic field, this gauge can be accepted as a fair approximation in the framework of the self-consistent calculations.

Further, let us perform transformation[14,15] of Eqs. (1), (2) to dimensionless variables. The temperature dependences of the coherence length $\xi(T)$, the magnetic field penetration depth $\lambda(T)$, as well as the coefficient a are the following:

$$\xi = \xi_0\left(1 - \frac{T}{T_c}\right)^{-1/2}, \quad \lambda = \lambda_0\left(1 - \frac{T}{T_c}\right)^{-1/2},$$

$$a = a_0\left(1 - \frac{T}{T_c}\right) \tag{22}$$

with the coefficients

$$\xi_0 = \frac{\hbar}{\sqrt{2m|a_0|}}, \quad \lambda_0 = \sqrt{\frac{mc^2 b}{16\pi e^2 |a_0|}}, \quad H_c = \sqrt{\frac{4\pi a_0^2}{b}}. \tag{23}$$

The GL parameter is defined as $\kappa = \lambda/\xi$. The transformed functions and variables become

$$\psi' = \frac{\psi}{\sqrt{|a_0|/b}}, \quad H' = \frac{H_z}{H_c}, \quad x' = \frac{x}{\lambda_0}, \quad y' = \frac{y}{\lambda_0}. \tag{24}$$

Further on, the primes will be omitted.

The order parameter ψ is a complex-valued function of coordinates and can be presented in a general form as

$$\psi(x,y) = \psi_a(x,y) e^{i\phi(x,y)}. \tag{25}$$

Substituting Eqs. (21)–(25) for the GL equations (1), (2), we obtain the following set of equations to determine $\psi_a(x,y)$, $\phi(x,y)$, and $H(x,y)$:

$$\frac{\partial^2 \psi_a(x,y)}{\partial^2 x} + \frac{\partial^2 \psi_a(x,y)}{\partial^2 y} - \left\{ \left(\frac{\partial \phi(x,y)}{\partial x}\right)^2 + \left(\frac{\partial \phi(x,y)}{\partial y}\right)^2 + \frac{\kappa}{\sqrt{2}} H(x,y)\left[y\frac{\partial \phi(x,y)}{\partial x} - x\frac{\partial \phi(x,y)}{\partial y}\right] + \kappa^2\left[-\left(1 - \frac{T}{T_c}\right) + \frac{1}{8}H^2(x,y)(x^2+y^2) + \psi_a^2(x,y)\right]\right\}\psi_a = 0, \tag{26}$$

$$\frac{\partial^2 \phi(x,y)}{\partial x^2} + \frac{\partial^2 \phi(x,y)}{\partial y^2} + 2\left[\frac{\partial \phi(x,y)}{\partial x}\frac{\partial \psi_a(x,y)}{\partial x} + \frac{\partial \phi(x,y)}{\partial y}\frac{\partial \psi_a(x,y)}{\partial y}\right] + \frac{\kappa}{\sqrt{2}} H(x,y)\left[y\frac{\partial \psi_a(x,y)}{\partial x} - x\frac{\partial \psi_a(x,y)}{\partial y}\right] = 0, \tag{27}$$

$$\frac{\partial^2 H(x,y)}{\partial x^2} + \frac{\partial^2 H(x,y)}{\partial y^2} - \frac{2\sqrt{2}}{\kappa}\psi_a(x,y)\left[\frac{\partial \psi_a(x,y)}{\partial y}\frac{\partial \phi(x,y)}{\partial x} - \frac{\partial \psi_a(x,y)}{\partial x}\frac{\partial \phi(x,y)}{\partial y}\right] - \psi_a(x,y)H(x,y)\left[x\frac{\partial \psi_a(x,y)}{\partial x} - y\frac{\partial \psi_a(x,y)}{\partial y}\right] - \psi_a^2(x,y)H(x,y) = 0. \tag{28}$$

It should be noted that the rigorous boundary condition for the magnetic field outside the loop is defined at infinity:

$$H(x,y)|_{x,y\to\infty}=H_0.$$

Assuming that the applied magnetic field H_0 does not change when approaching the sample up to its surface from outside, the set of the boundary conditions at the external boundary results:

$$\left.\frac{\partial\psi_a(x,y)}{\partial x}\right|_{\text{ext, } x=\text{const}}=0,\quad \left.\frac{\partial\psi_a(x,y)}{\partial y}\right|_{\text{ext, } y=\text{const}}=0,$$

$$\left.\left(\frac{\partial\phi(x,y)}{\partial x}+\frac{\kappa}{2\sqrt{2}}H_0y\right)\right|_{\text{ext, } x=\text{const}}=0,$$

$$\left.\left(\frac{\partial\phi(x,y)}{\partial y}-\frac{\kappa}{2\sqrt{2}}H_0x\right)\right|_{\text{ext, } y=\text{const}}=0,$$

$$H(x,y)|_{\text{ext}}=H_0. \tag{29}$$

Similarly, for the internal boundary it follows that

$$\left.\frac{\partial\psi_a(x,y)}{\partial x}\right|_{\text{int, } x=\text{const}}=0,\quad \left.\frac{\partial\psi_a(x,y)}{\partial y}\right|_{\text{int, } y=\text{const}}=0,$$

$$\left.\left(\frac{\partial\phi(x,y)}{\partial x}+\frac{\kappa}{2\sqrt{2}}H_iy\right)\right|_{\text{int, } x=\text{const}}=0,$$

$$\left.\left(\frac{\partial\phi(x,y)}{\partial y}-\frac{\kappa}{2\sqrt{2}}H_ix\right)\right|_{\text{int, } y=\text{const}}=0,$$

$$H(x,y)|_{\text{int}}=H_i. \tag{30}$$

The magnetic field inside the opening H_i depends on the applied magnetic field H_0 and can be determined from the integral relation (see Ref. 16 and the Appendix)

$$\frac{c}{4\pi}\oint_i \text{rot }\mathbf{H}\cdot d\,\mathbf{l}-\frac{c}{4\pi\lambda^2}(\Phi_f-\Phi_i)=0, \tag{31}$$

with the condition of the fluxoid quantization

$$\Phi_f=L\Phi_0,\quad L=0,\ 1,\ 2,\ldots\ . \tag{32}$$

Here $\Phi_0=ch/2e$ is the flux quantum and $\Phi_i=\oint_i\mathbf{A}\cdot d\,\mathbf{l}$ is the magnetic flux through the opening of the loop. The integration runs over the internal boundary of the loop.

The self-consistent procedure of finding the solutions implies, first, that the obtained distributions $H(x,y)$, $\psi_a(x,y)$, and $\phi(x,y)$ should satisfy all the equations of the boundary problem simultaneously and, second, that the value of the magnetic field inside the opening H_i of the loop should obey the integral relation (31). The calculation of the integral entering Eq. (31) requires the knowledge of the magnetic field $H(x,y)$ distribution which can be found only self-consistently with $\psi_a(x,y)$ and $\phi(x,y)$. In their turn, the boundary conditions for $H(x,y)$ and $\phi(x,y)$ themselves depend on H_i. Therefore, adjusting the magnetic field in the opening of the loop H_i to the applied magnetic field H_0 in order to fulfill condition (31), we obtain the problem with new boundary conditions. Thus, when solving the set of equations (26)–(32) one faces a nonlinear multiparameter problem which includes a set of nonlinear partial differential equations and an integral equation (31).

Equations (26)–(28) with boundary conditions (29), (30) together with relation (31) are solved numerically by using the finite-difference method for partial differential equations.[18] For the numerical solution, we have used a rectangular grid which contains 241 points in the direction of leads and 121 points in the perpendicular direction. Every single equation is solved by the multiple subsequent passing through all the points of the grid until the distribution of the sought quantity does not change anymore. Then the obtained distribution of the given quantity [$H(x,y)$, $\phi(x,y)$, or $\psi_a(x,y)$] is used for all the other equations with the corresponding boundary conditions. This iteration procedure is continued as many times as it is necessary in order to obtain a self-consistent solution. Our estimations show that it is enough to perform about 6000 iterations to provide the relative accuracy 10^{-4} of the solution of the set of equations (26)–(30) for a given trial value of H_i. In practice, we used the number of iterations 10 000. After this solution is obtained, condition (31) is examined. If it is not fulfilled, the next round of calculations is necessary. This procedure is repeated until condition (31) is satisfied with the guaranteed accuracy of 1%. Typically, 10–20 rounds of calculations are required depending on the choice of the initial trial value of H_i.

IV. SOLUTIONS OF GINZBURG-LANDAU EQUATIONS FOR A SQUARE LOOP WITH LEADS

In this section, we discuss typical features of the obtained solutions of the GL equations, i.e., of the distributions of the magnetic field $H(x,y)$, the phase $\phi(x,y)$, and the squared amplitude $\psi_a^2(x,y)$ of the order parameter, for the mesoscopic square loop with leads.

A. Examples of the distributions

The examples of typical distributions of the magnetic field $H(x,y)$, the phase of the order parameter $\phi(x,y)$, and its squared amplitude $\psi_a^2(x,y)$ are presented in Fig. 3. As convenient units for T and H the following values are chosen: the critical temperature at zero magnetic field $T_c(H=0)\equiv T_c$ (the Ginzburg-Landau critical temperature, $T_c=1.2$ K for Al) and the critical magnetic field for bulk Al at zero temperature $H_c(T\to 0)=100$ G (cf. Ref. 17). Increasing the temperature from $T/T_c(0)=0.8$ [Fig. 3(a)] to $T/T_c(0)=0.94$ [Fig. 3(b)] at a fixed value of the applied magnetic field $H_0=0.1H_c(0)$ leads to a substantial (approximately, by a factor of 5) suppression of $\psi_a^2(x,y)$ everywhere in the

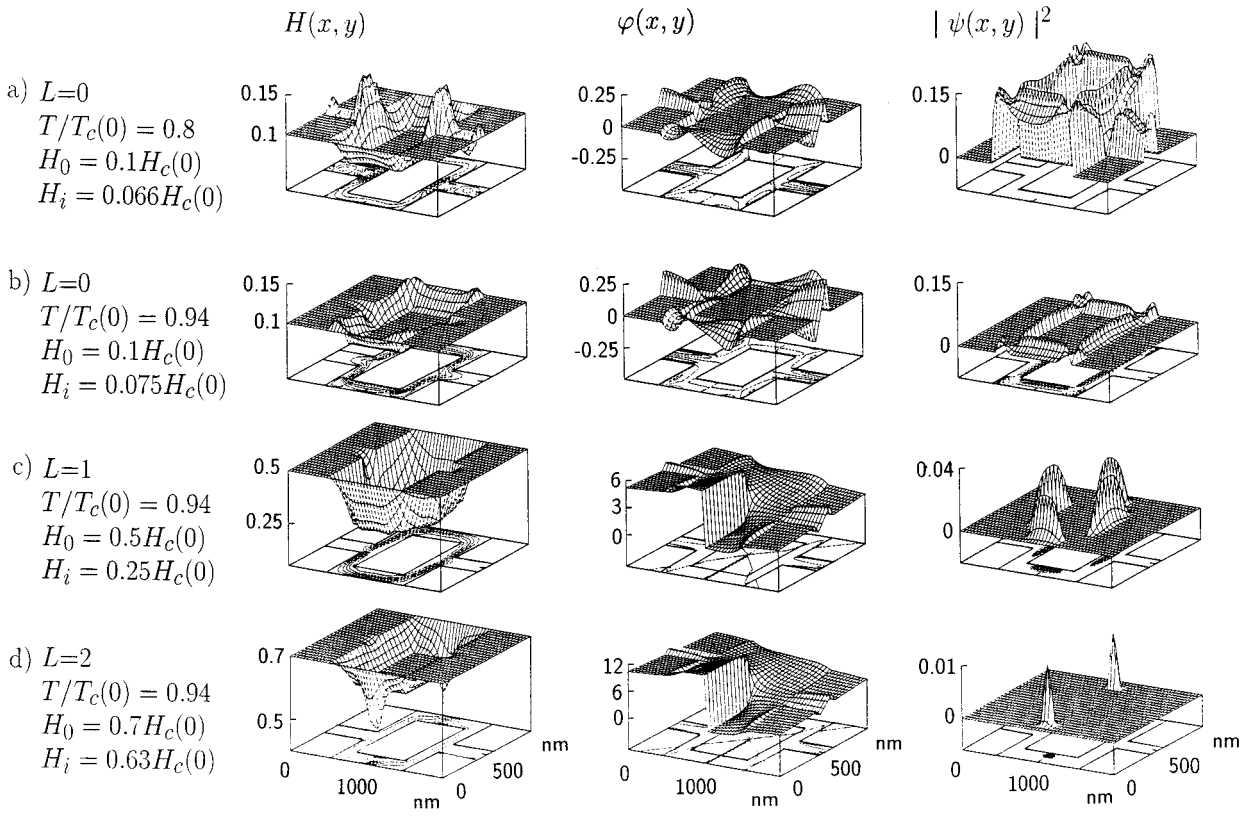

FIG. 3. Calculated distributions of the magnetic field $H(x,y)$, the phase of the order parameter $\phi(x,y)$, and its squared amplitude $\psi_a^2(x,y)$ in a mesoscopic square loop with leads. As a unit for $H(x,y)$, the critical magnetic field for bulk Al at zero temperature is used: $H_c(T\rightarrow 0)=100$ G; $\psi_a^2(x,y)$ is measured in units $|a_0|/b$, where a_0 and b are the GL parameters.

structure with a simultaneous concentration of the order-parameter around the opening and in the corners of the loop. The phase of the order parameter $\phi(x,y)$ for $L=0$ has an oscillatory behavior. The modulation of the magnetic field $H(x,y)$ is stronger in the case of an intensive distribution of the order parameter at the lower temperature and is weaker in the case of the higher temperature when the order-parameter distribution has a much lower magnitude. The aforementioned increase of temperature leads to a small change of the magnetic field inside the opening from the value $H_i=0.066H_c(0)$ to $H_i=0.075H_c(0)$.

For higher applied magnetic fields [Figs. 3(c) and 3(d)] it is favorable for the superconducting loop, to capture some number of the flux quanta according to the condition of the magnetic flux quantization (32). Increase of the magnetic flux number from $L=0$ [Fig. 3(b)] to $L=1,2$ (Figs. 3(c) and 3(d)] at a fixed temperature leads to a considerable suppression of the order parameter and to the localization of the superconducting phase ''islands'' near the midpoints of the internal sides of the loop. The distribution of $\phi(x,y)$ keeps an oscillating character but for $L\neq 0$ the trace along any closed path around the loop results in the *phase shift* $2\pi L$.

B. The influence of leads on the distributions of the order parameter and the field in the loop

For the structures under consideration, when the width of the loop and leads relates to the external side of the loop as 1.5:10, it is revealed that the presence of leads does not affect strongly the magnetic field and the order-parameter distributions in the loop itself. Leads weakly distort the patterns of the distributions, which obey the C_4 symmetry peculiar for an isolated square loop, reducing their symmetry to C_2. As shown in Fig. 4, for the particular case $T/T_c(0)=0.6$, $H_0=0.4H_c(0)$, $L=0$ there are maxima in the $\psi_a^2(x,y)$ distribution at the links of leads to the loop. Such maxima are absent at the corresponding points of the $\psi_a^2(x,y)$ distribution in the adjacent sides. These results are in agreement with the analysis in the framework of the network model which gives a stronger order parameter at the nodes.[19] Simultaneously, the maxima in the $H(x,y)$ distribution near the midpoints of the external sides of the loop are destroyed by leads. Shortening the leads from $Q_l=0.5Q_e$ to $Q_l=0.25Q_e$ does not result in any visible change of the magnetic field and the order-parameter distributions in the body of the loop. For the case of leads with a length much smaller than the side of the loop, $Q_L=0.08Q_e$, the features of $H(x,y)$ and $\psi_a^2(x,y)$ distributions typical for corners appear in the vicinity of the links. In an isolated loop, the distributions of the magnetic field and the order parameter acquire the C_4 symmetry.

C. The evolution of the $\psi_a^2(x,y)$ distribution in the loop

In order to follow up the evolution of the ''islands'' of the superconducting phase in the loop for a certain fixed orbital number L, we will change the applied magnetic field H_0 from the value which corresponds to the appearance of nonzero $\psi_a^2(x,y)$ [according to the accuracy of the calculations,

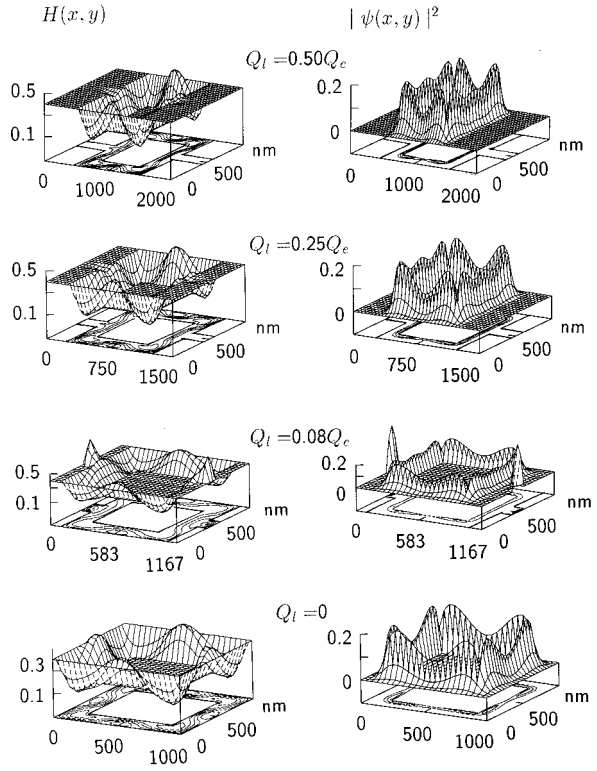

FIG. 4. Influence of the width of leads Q_l on the distributions of the magnetic field and the order parameter in the loop. The units for the magnetic field $H(x,y)$ and for the squared amplitude of the order parameter $\psi_a^2(x,y)$ are the same as those in Fig. 3.

the value $\psi_a^2(x,y) > 10^{-6}$ is treated as nonzero] in the structure up to the value at which the superconductivity disappears. The corresponding changes of the magnetic field in the loop, $H(x,y)$, and the squared amplitude of the order parameter, $\psi_a^2(x,y)$, are represented in Fig. 5(a). The peaks of the superconducting phase at $T/T_c(0) = 0.94$ for $L = 1$ originate in the corners of the loop at low applied magnetic field. Following condition (31), the magnetic field inside the opening is higher than the applied one: $H_i > H_0$. The increase of H_0 leads to a nonmonotonous distribution of magnetic field $H(x,y)$ in the leads and to the increase of H_i. These changes are accompanied (i) by the appearance of the superconducting phase in the leads and by the growth of the amplitude of $\psi_a^2(x,y)$ in the corners; (ii) by broadening and splitting of the peaks of $\psi_a^2(x,y)$ in the corners followed by their motion towards the midpoints of the external sides of the loop. The further increase of the applied magnetic field leads to dramatic changes of $H(x,y)$ and $\psi_a^2(x,y)$. In contrast to the growth of H_i consistently with the growth of the applied magnetic field at lower H_0, the magnetic field in the opening starts to decrease and at a certain value of H_0 becomes equal to it: $H_i = H_0$. The respective picture of $\psi_a^2(x,y)$ is characterized by the formation of the superconducting ''islands'' near the midpoints of the external sides of the loop and the ''leakage'' of $\psi_a^2(x,y)$ towards the midpoints of internal sides. If the increase of H_0 is continued, H_i diminishes and becomes lower than H_0. The superconducting ''islands'' concentrate near the midpoints of the internal sides of the loop and then disappear.

It is worth noting that for a certain range of values of the applied magnetic field [$H_0 \leqslant 0.1H_c(0)$ for $L = 1$] the distribution of the order parameter in each corner of a mesoscopic superconduncting loop clearly reveals nucleation of the superconducting phase in the vicinity of the corners. Such a behavior of the superconducting order parameter has been anticipated by a corresponding distribution obtained within the simple model of an *isolated* corner analyzed in Sec. II, as is obvious from Fig. 5(b). When further increasing the applied magnetic field, the distribution of the order parameter is determined to a decisive measure by the geometry of the mesoscopic superconducting structure *as a whole*.

The above analysis of the evolution of the ''superconducting islands'' has shown that, along with smooth spatial changes of the order parameter, sharp inhomogeneities are also possible when the ''islands'' turn themselves into peaks of $\psi_a^2(x,y)$. The relative status of these two kinds of inhomogeneities will now be clarified. According to the relation between the characteristic length of inhomogeneity of the order parameter, i.e., the typical distance over which the ψ changes, on the one hand, and ξ_0 or $\xi(T)$, on the other hand, inhomogeneities can be classified into two kinds. We call those whose characteristic lengths are of the order of or smaller than ξ_0 [$\xi(T)$] and larger than ξ_0 [$\xi(T)$] ''short-range'' and ''long-range'' inhomogeneities, respectively. The temperature-dependent coherence length $\xi(T)$ is a monotonously increasing function [see Eqs. (22)]. Therefore, at an arbitrary nonzero T, $\xi(T) > \xi_0$. For instance, at $T/T_c = 0.6$, $\xi(T) = 158$ nm. At higher temperatures, we have $\xi(T) = 223$ nm at $T/T_c = 0.8$, and at $T/T_c = 0.94$ $\xi(T) = 408$ nm. Hence, even at relatively high temperatures, inhomogeneities of ψ along the side of the loop (1000 nm) and those along the leads (500 nm) are of the ''long-range'' kind. In most cases, the distributions presented in Figs. 3–5(a) are examples of such inhomogeneities. The ''long-range'' changes of ψ across the side of the loop are possible at relatively low temperatures.

Though formally, the ''short-range'' changes could be treated by adding an extra gradient term into GL equations (see Ref. 12), these inhomogeneities are not excluded from the present analysis. In our opinion, the reason to retain them in the present consideration is the following. In the previous subsection, we traced the evolution of the ''islands'' of the superconducting phase. It was seen how the ''islands'' move inside the loop as well as how they appear, grow, and disappear. The ''long-range'' changes continuously turn into the ''short-range'' changes and vice versa. Therefore, the ''short-range'' inhomogeneities, or peaks of the superconducting phase, which appear as a result of this evolution, have at least qualitative or *extrapolative* meaning. For example, the peaks of ψ have been plotted in Fig. 3(d) to illustrate a continuous character of the evolution of the ψ distribution with increasing applied magnetic field [cf. Fig. 3(c)] up to disappearance of the superconducting phase. The qualitative picture of the evolution of the order-parameter distribution, resulting from Fig. 5(a), will be used below for the illustration of different criteria to define the phase boundary.

D. The thermodynamical stability of the solutions

In a previous paper,[20] approximate equations based on the assumption of slowly varying amplitude of the order param-

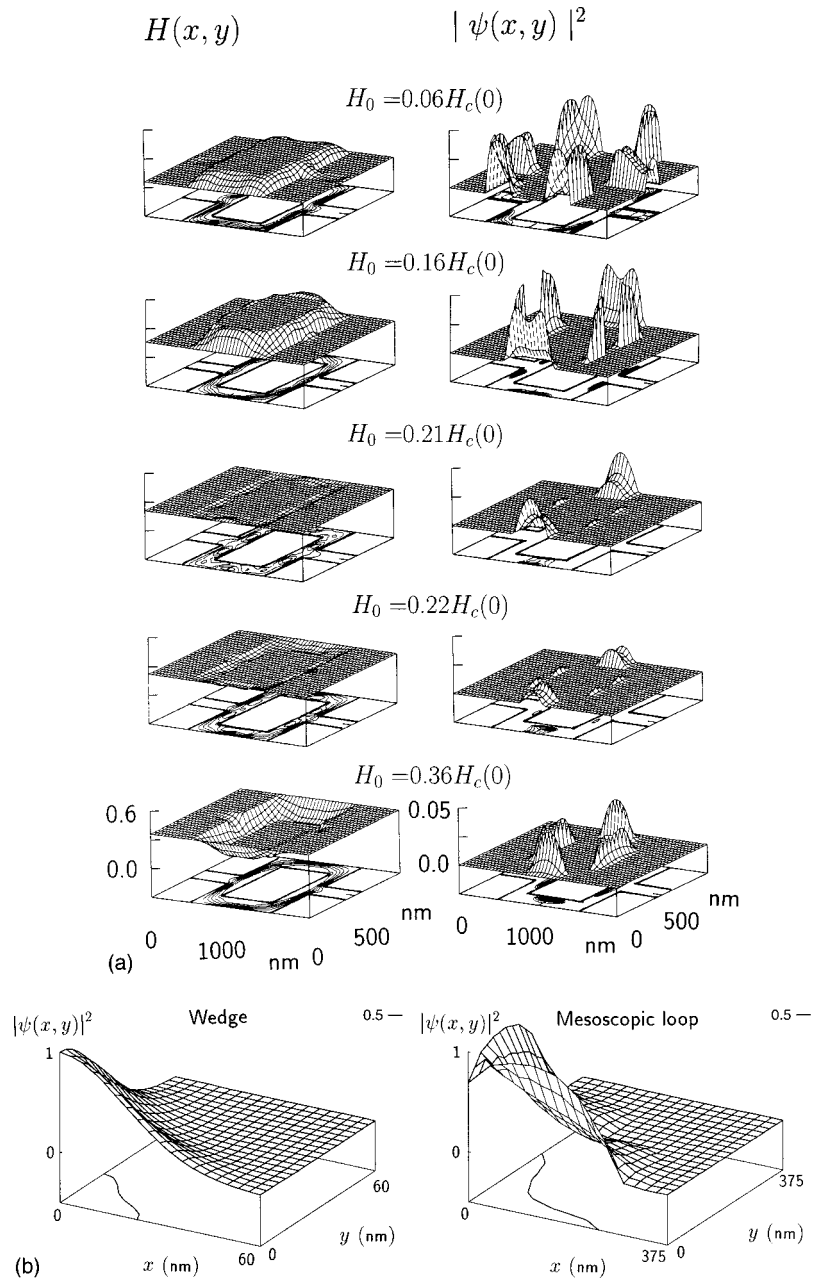

FIG. 5. (a) Evolution of the ''islands'' of the superconducting phase in the loop for a fixed orbital number $L=1$: (i) $H_0=0.06H_c(0)$, $H_i>H_0$, appearance, broadening and splitting of the peaks of $\psi_a^2(x,y)$ in the corners; (ii) $H_0=0.16H_c(0)$, $H_i>H_0$, motion of the ''islands'' of the superconducting phase towards the midpoints of the external sides of the loop; (iii) $H_0=0.21H_c(0)$, $H_i=H_0$, confluence of the ''islands'' of the superconducting phase near the midpoints of the external sides and starting of their ''leakage'' towards the midpoints of the external sides; (iv) $H_0=0.22H_c(0)$, a thermodynamically stable state, $H_i<H_0$, continuation of the ''leakage'' of the superconducting phase from the midpoints of the external sides to those of the internal sides; (v) $H_0=0.36H_c(0)$, a stable state, $H_i<H_0$, concentration of the ''islands'' near the midpoints of the internal sides of the loop, disappearance of the superconducting phase in the loop. (b) Comparison between the distributions of the order parameter in the wedge (as obtained in Sec. II; the left-hand panel) and in a corner of the superconducting loop for $L=1$ (shown magnified in the right-hand panel) at $H_0=0.06H_c(0)$.

eter as compared to the phase changes, were used instead of the full set of equations (26)–(28) for $H(x,y)$, $\phi(x,y)$, and $\psi_a(x,y)$ of the present paper. The comparison of the solutions obtained in both cases shows that there is a fair qualitative and quantitative agreement between corresponding solutions for $\phi(x,y)$ and $\psi_a(x,y)$ in both approaches for the H-T points in the vicinity of the phase boundary.

However, the simplified approach of Ref. 20 is less detailed than the present paper and it has not allowed us to analyze the essential features of the evolution of the order parameter in the loop. As an example, it could not reveal the ''leakage'' of the superconducting phase between the midpoints of the external and internal sides of the loop. Also, for the purpose of the determination of characteristics of the superconducting states such as free energy or magnetization far away from the phase boundary, the exact equations (26)–(28) are necessary because they take into account the magnetic field modulations inside the structure.

The free energy per unit of the volume of the superconductor in the magnetic field is[14]

$$F_{sH}=F_{n0}+a|\psi|^2+\frac{b}{2}|\psi|^4+\frac{H^2}{8\pi}+\frac{1}{2m}\left|-i\hbar\nabla\psi-\frac{2e}{c}\mathbf{A}\psi\right|^2, \tag{33}$$

where F_{n0} is the free energy of the normal (nonsuperconducting) phase. For type-II superconductors ($a<0$), only the second term in the right-hand side of Eq. (33) reduces the free energy of the sample in the superconducting state. All the other terms, which are related to the order parameter, can lead only to increase in F_{sH} (cf. Ref. 21). Consequently, the term which contains the value of the magnetic field is of importance for minimization of F_{sH}. Due to the fact that the magnetic field inside the opening H_i differs from the applied magnetic field H_0, one should take into account the contribution to the free energy related to this difference. So, it is obvious that those states are expected to provide the minimal value of the free energy which are accompanied by a reduction of the magnetic field in the opening of the loop. This is confirmed by the numerical calculations of the free energy. In particular, for the parameters corresponding to Fig. 5(a) [$L=1$, $T/T_c(0)=0.94$] we have found that only those states are thermodynamically stable, i.e., correspond to the minimum of the free energy, which are obtained at the applied magnetic field ranging between $H_0\approx 0.19H_c(0)$ and $0.38H_c(0)$. For this range, H_i is less than, or nearly equal to, H_0. For lower applied magnetic fields, the states with nonzero $\psi_a^2(x,y)$ at $L=1$ occur to be thermodynamically unstable: the minimum of the free energy is at $L=0$. For higher magnetic fields, the states with $L>1$ are preferable.

We have plotted schematically the regions of the thermodynamically stable states for different values of L for the superconducting loop under consideration (Fig. 6). Every curve represents the boundary between the superconducting and the normal states for a certain number L. The envelope of all the curves forms, obviously, the H-T phase boundary which includes parts related to different numbers L according to the requirement of the thermodynamical stability. As it it seen from Fig. 6, in the areas where the superconducting states with different numbers L are possible, such a state occurs to be thermodynamically stable, which corresponds to the minimal number L.

It should be noted that we have not specified here the criterion to determine the phase boundary. It will be shown in the next section that the phase boundary strongly depends on the definition of such a criterion.

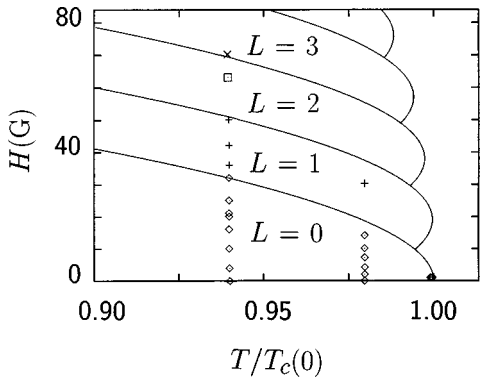

FIG. 6. Regions of the thermodynamically stable states with different L for the superconducting loop: the examples of the stable states are plotted for $L=0$ ($\diamond$), $L=1$ ($+$), $L=2$ ($\square$), $L=3$ ($\times$).

V. EQUILIBRIUM SUPERCONDUCTING STATES: THE H-T SUPERCONDUCTING PHASE BOUNDARY

A. Inhomogeneous distribution of the order parameter

The above analysis shows that for all considered cases the distribution of the order parameter $\psi_a^2(x,y)$ in the loop is inhomogeneous. Moreover, the areas where $\psi_a^2(x,y)=0$ can coexist with the ones with $\psi_a^2(x,y)\neq 0$. This inhomogeneity appears as a consequence of the interplay between the C_4 symmetry of the loop (reduced to the C_2 symmetry by leads) and the cylindrical symmetry of the magnetic field. The order-parameter distributions reveal the local features, which are remarkable in the neighborhood of the midpoints of the internal sides and in the corners of the loop, in correspondence with the analytical results discussed in Sec. II.

Note that in the case of a circular loop the magnetic field and the loop have the same symmetry, and as a result the order-parameter distribution can display inhomogeneity only in the *radial* direction. This result refers, of course, to the case of an *ideal* circular loop having a constant width. Recent analysis[22] performed for a cylinder with average radius R and *nonuniform* width $D(\theta)$, where θ is the azimuthal angle, has demonstrated the angular dependence of the order-parameter distribution in the sample.

In contrast to the case of a circular loop, an obvious consequence of the inhomogeneous distribution of $\psi_a^2(x,y)$ in the square loop is the fact that in different parts of the loop the order parameter disappears at various values of the applied magnetic field for a given temperature, or at various temperatures for a given applied magnetic field.

Therefore, for different parts of the loop, one has different values of the critical magnetic fields $H_{c,n}$ and temperatures $T_{c,n}$. Which of them should be chosen as those characterizing the loop as a whole? At first sight, it seems to be natural to use the *maximal* values of $H_{c,n}$, $T_{c,n}$ for this purpose, i.e., to treat the *total* suppression of the superconductivity in *all* parts of the loop as a criterion for the phase boundary point. However, such an analysis shows (see also Ref. 20) that the phase boundary calculated using the criterion of the total suppression of the superconducting phase in the loop would be in disagreement with the experimental results.[4] This is due to the fact that the phase boundary in Ref. 4 has been reconstructed by measuring the temperature shift of the midpoint of the normal-to-superconducting resistive transition as a function of the applied magnetic field. This corresponds to the existence of a certain ''filling'' of the loop by the superconducting phase which provides the resistivity of the sample equal to a half of its value in the normal state. Obviously, if one determines experimentally the phase boundary based on the criterion of the *total* suppression of the superconductivity, one should measure the temperature shift of the beginning of the normal-to-superconducting resistive transition (which is close to the resistivity of the normal phase). Therefore, another criterion should be chosen for phase boundary points in order to explain the H-T phase boundary obtained in Ref. 4.

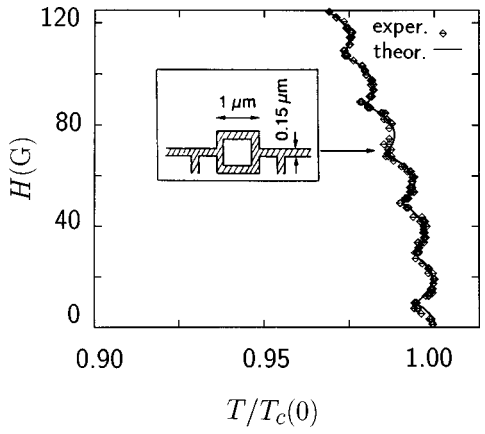

FIG. 7. The *H-T* phase boundary: experimentally detected in Ref. 4 by measuring the temperature shift of the midpoint of the normal-to-superconducting resistive transition ($\diamond$) and calculated using the criterion of the ''appearance of the superconducting path'' between the leads of the loop (solid line).

For the purpose of the quantitative description of different phase boundary criteria, we introduce the ''filling parameter'' defined as a ratio of the area of the loop in which the squared amplitude of the order parameter is nonzero (in our calculations: larger than 10^{-6}) to the total area of the loop:

$$\eta = \frac{S(\psi_a^2(x,y)>0)}{S_{\text{loop}}}. \tag{34}$$

For example, $\eta=0$ corresponds to the total suppression of the superconductivity in the loop.

If one attempts to model the experimental conditions of Ref. 4 using the value $\eta=0.5$, the calculated phase boundary has the period of oscillations which is approximately twice smaller than experimentally observed one. This has been demonstrated in Ref. 20 for the loop without leads. The analysis of the distributions of $\psi_a^2(x,y)$ shows that for $\eta=0.5$ there exists a single-connected area with nonzero $\psi_a^2(x,y)$ between the leads of the loop which will be referred to as a ''*superconducting path.*'' If there exists a well-developed ''superconducting path,'' electronic motion along this part of the loop occurs without any resistance, although the loop contains the normal phase in some parts. So, for weak currents, $\eta=0.5$ corresponds rather to a point of the normal-to-superconducting resistive transition in the vicinity of zero resistivity, than to the midpoint.

Therefore, in order to model the experimental conditions of Ref. 4, one should use some value of η from the range 0–0.5. The detailed analysis of $\psi_a^2(x,y)$ distributions for certain numbers L at different values of the applied magnetic field [Fig. 5(a)] shows that at low magnetic fields, the areas in the corners of the loop contain the superconducting phase. These areas do not contribute to the ''superconducting path.'' At the same time, the value of η substantially depends on whether the areas in the corners are filled with the superconducting or with the normal phase. In order to describe the same ''superconducting path'' for different values of H_0 excluding the contributions to η from the areas in the neighborhood of the corners, one should choose different values of η.

As seen from Fig. 7, a good agreement between the theoretical results for the superconducting phase boundary in the Al mesoscopic square loop and the experimental data of Ref. 4 is achieved when there are still small spacings filled with the normal phase between the islands of the superconducting phase. This situation can be regarded as the ''appearance of the superconducting path.'' Due to the spacings, the resistivity of the loop measured between the leads occurs nearly twice smaller than that for the normal phase. In such a way, the criterion of the ''appearance of the superconducting path'' between the leads of the loop corresponds, for the calculation of the phase boundary, to the experimental conditions of measuring the temperature shift of the midpoint of the normal-to-superconducting resistive transition. The calculations show that this criterion is satisfied for the values $\eta \approx 0.04-0.1$.

For the purpose of calculations of the boundaries between the areas of the superconducting states with different numbers L in Fig. 6 (subsection IV D), the criterion of the ''appearance of the superconducting path'' has been also used.

B. Uniform amplitude of the order parameter within the GL equations

As shown in Sec. IV, the ''short-range'' inhomogeneities of the order parameter appear predominantly in the vicinity of the phase boundary. In order to investigate whether or not the phase boundary substantially depends on inhomogeneities of this kind, the problem is analyzed here in the limit of a uniform amplitude of the order parameter.

We will treat this problem in the strict sense of the London limit in the next subsection. Here, we consider an approach which still keeps features of the above treatment in the framework of GL equations, namely, a self-consistent determination of ψ_a^2.

To comply with the requirement that the amplitude of the order parameter be a constant, we put

$$\frac{\partial \psi_a(x,y)}{\partial x} = \frac{\partial \psi_a(x,y)}{\partial y} = 0 \tag{35}$$

in the GL equations (27)–(28), as well as in the boundary conditions (29)–(30) and in the integral relation (31). Then the following set of equations is obtained to determine $\phi(x,y)$ and $H(x,y)$:

$$\frac{\partial^2 \phi(x,y)}{\partial x^2} + \frac{\partial^2 \phi(x,y)}{\partial y^2} = 0, \tag{36}$$

$$\frac{\partial^2 H(x,y)}{\partial x^2} + \frac{\partial^2 H(x,y)}{\partial y^2} - \psi_a^2 H(x,y) = 0. \tag{37}$$

The squared amplitude of the order parameter ψ_a^2 enters Eq. (37) as a parameter. To determine this parameter, we solve Eq. (26) together with Eq. (35) with respect to ψ_a^2 and then average the obtained value over the loop:

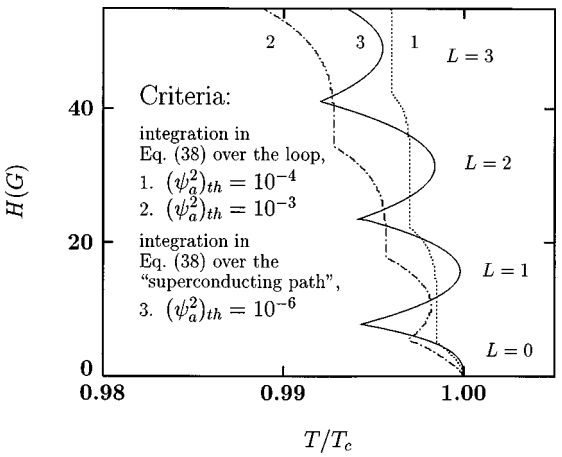

FIG. 8. The H-T phase boundaries calculated using the approximation of a homogeneous amplitude of the order parameter within the GL equations for $L=0,\ 1,\ 2,\ 3$ by different criteria: suppression of the superconducting phase in the loop, the threshold value $(\psi_a^2)_{th}=10^{-4}$ (curve 1), $(\psi_a^2)_{th}=10^{-3}$ (curve 2); total suppression of the superconducting phase in the ''superconducting path,'' $(\psi_a^2)_{th}=10^{-6}$ (curve 3).

$$\overline{\psi_a^2}=\frac{1}{S_{\rm loop}}\int_{\rm loop}\left\{\left(1-\frac{T}{T_c}\right)-\frac{1}{8}H^2(x,y)(x^2+y^2)\right.$$
$$-\frac{1}{\kappa^2}\left[\left(\frac{\partial\phi(x,y)}{\partial x}\right)^2+\left(\frac{\partial\phi(x,y)}{\partial y}\right)^2\right]$$
$$\left.-\frac{1}{\kappa\sqrt{2}}H(x,y)\left[y\frac{\partial\phi(x,y)}{\partial x}-x\frac{\partial\phi(x,y)}{\partial y}\right]\right\}dxdy. \tag{38}$$

Equations (36)–(38) are solved as follows. First, we solve Eq. (36) imposing the appropriate boundary conditions by the numerical methods described in Sec. III. Second, a self-consistent solution of Eqs. (37), (38) is derived, also with the corresponding boundary conditions. Namely, we obtain $\overline{\psi_a^2}$ from Eq. (38) and then use this value as the parameter ψ_a^2 entering Eq. (37). These calculations are repeated until the integral relation (31) is fulfilled.

In such a way, the present approach combines, on the one hand, the requirement that the order-parameter amplitude be a constant and, on the other hand, a self-consistent procedure of calculation of ψ_a^2, borrowed from the GL equations (26)–(28).

As a result of this procedure, another set of phase boundaries is obtained, which are plotted in Fig. 8 for $L=0,\ 1,\ 2,\ 3$. These phase boundaries have the quasioscillating Little-Parks-type behavior and differ from each other by the average slope of the envelope and by the period of oscillations, depending on a specific criterion, chosen to determine a phase boundary. We establish different threshold values of the $(\psi_a^2)_{th}$ as criteria of the phase boundary. Curve 1 corresponds to $(\psi_a^2)_{th}=10^{-4}$, curve 2 corresponds to $(\psi_a^2)_{th}=10^{-3}$. To define the criterion, which correlates to the criterion of the ''appearance of the superconducting path'' previously used in the case of the inhomogeneous ψ_a^2 distribution (subsection V A), the integration in the right-hand side of Eq. (38) can be performed over the ''superconducting path.'' This area is simulated by the geometrical figure which overlaps the square loop under consideration, except the external boundary, which is formed by the parts of the circle inserted in the loop; a radius of the circle is $[(Q_e/2)^2+(d/2)^2]^{1/2}$. The phase boundary calculated by the criterion of the total suppression of ψ_a^2 [according to the accuracy of the calculations, $(\psi_a^2)_{th}=10^{-6}$] over the ''superconducting path'' is represented by curve 3 in Fig. 8.

Comparison shows that these phase boundaries are similar to the previously calculated one in subsection V A, when the inhomogeneity of the order parameter was taken into account. The average slope of the envelope and the period of oscillations of the phase boundaries represented in Fig. 8 are close to these characteristics of the curve plotted in Fig. 7. Moreover, from the comparison of the phase boundary depicted in Fig. 7 with curves 1 and 2 in Fig. 8, which are obtained for the threshold values 10^{-4} and 10^{-3}, respectively, we can expect that there exists some intermediate threshold value $(\psi_a^2)_{th}$ between 10^{-4} and 10^{-3} which would provide also a quantitative agreement between phase boundaries calculated in the framework of the different approaches under discussion. At the same time, it is worth noting that there is a distinction in the shape of cusps forming the phase boundaries 1, 2 in Fig. 8 and the calculated phase boundary in Fig. 7. Every cusp, referred to a certain value of L, of the phase boundary represented in Fig. 7 has a shape close to symmetric with respect to the horizontal line guided through the central point of this cusp, and it is asymmetric for curves 1, 2 in Fig. 8. The noted difference is eliminated by performing the integration in Eq. (38) over the ''superconducting path.'' The corresponding curve 3 in Fig. 8 is formed by nearly symmetric cusps for every particular number L.

C. The London limit

In this subsection, we treat the phase boundary of the mesoscopic square loop under consideration in the London limit which is valid, in any case, when $T\to T_c$. In this limit, the parameter ψ_a^2 entering Eq. (37) is a constant which has the meaning of the inverse London penetration depth λ_L.[16] With the notations used in the present work, ψ_a^2 is related to the temperature-dependent penetration depth[16]

$$\lambda(T)=\lambda(0)\left(\frac{T_c(0)-T}{T_c(0)}\right)^{-1/2} \tag{39}$$

as

$$\psi_a^2=\frac{mc^2}{16\pi e^2\lambda^2(T)}. \tag{40}$$

In terms of the dimensionless variables (23)–(24), one obtains a simple dependence of ψ_a^2 on temperature:

$$\psi_a^2=1-\frac{T}{T_c(0)}. \tag{41}$$

Hence, $\phi(x,y)$ and $H(x,y)$ are determined by the set of equations (36), (37) with ψ_a^2 given by Eq. (41).

It is clear that, due to the fact that in the London limit ψ_a^2 is a certain constant at a given temperature, one can use no

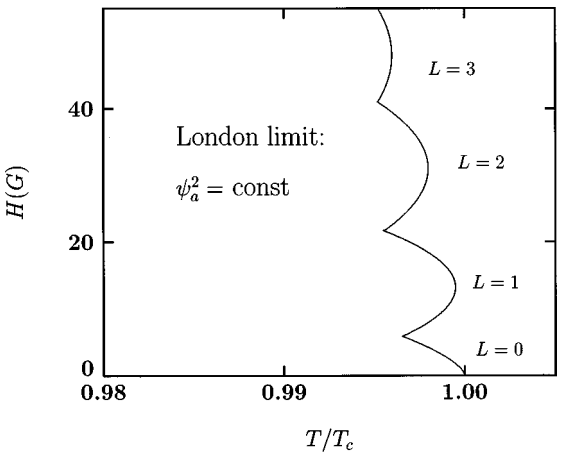

FIG. 9. The *H-T* phase boundary calculated in the London limit for $L=$ 0, 1, 2, 3 by the analysis of the Laplacian of the persistent currents in the loop (see discussion in the text).

threshold value of ψ_a^2 to define a criterion for the phase boundary, as distinct from subsections V A and V B. We have elaborated a method of the phase boundary calculation which is based on the analysis of the distributions of the persistent current in the square loop. The underlying idea of this method is the following. In the superconducting state, the current obeys the second London equation,[17] which corresponds to the Helmholtz equation. On the phase boundary, the second London equation formally turns to the Laplace equation. Therefore, the value of the Laplacian of the persistent current has to be analyzed in order to define the phase boundary between the superconducting and normal states.

It is worth recalling that, in the calculations of the phase boundary performed in the present work, we simulate the experimental data[4] on the midpoint of the normal-to-superconducting resistive transition. This was a reason to use some value of the ''filling parameter'' (subsection V A) or some threshold values of ψ_a^2 to determine the phase boundary (subsection V B). The same goal is pursued in the present consideration by choosing a threshold value of the Laplacian of the persistent current. For convenience, we use the Laplacian of the persistent current averaged over the area of the structure. As a threshold value, we choose 1% of its maximum obtained at a fixed temperature for those values of the applied magnetic field, which are compatible with a given number L. (A detailed description of the calculations of persistent current in a square loop as well as different criteria of the phase boundary will be done elsewhere.) The resulting phase boundary is represented in Fig. 9.

From the analysis performed in this section, a general conclusion follows: the phase boundaries are not strongly sensitive to the specific features of the order-parameter distributions ψ_a^2 which have been defined as the ''short-range'' inhomogeneities. Different approaches used in this section lead to similar phase boundaries for the mesoscopic superconducting square loop, which agree with the available experimental data. At present, we are not aware of any direct experimental study of the *local* distributions of the magnetic field and the order parameter in a square mesoscopic loop. If a distribution of the order parameter occurs to be inhomogeneous in a mesoscopic structure, in particular, in the square loop under discussion, then the theoretical approach which has been developed in subsection V A of the present paper can be applied for the description of such a structure. On the contrary, in the case where the order parameter is nearly homogeneous in a particular structure, another approach, which has been represented in subsections V B and V C, is relevant. The present investigation has been carried out for both of these two different regimes.

VI. CONCLUSIONS

The problem of the *H-T* phase boundary in superconducting loops is discussed in detail.

The study of the phase boundary of a superconductor filling a wedge with the central angle α is performed in terms of a variational model based on the linearized GL theory and for a uniform magnetic field. The obtained solutions imply that the nucleation of the superconducting phase in the corner is enhanced in the vicinity of the edge when $0<\alpha<\pi$.

A self-consistent solution of the GL equations for a mesoscopic square superconducting loop with the appropriate boundary conditions is obtained numerically. The distributions of the magnetic field $H(x,y)$, the squared amplitude $\psi_a^2(x,y)$, and the phase $\phi(x,y)$ of the order parameter are found for the cases when an enclosed fluxoid contains a different number L of magnetic flux quanta Φ_0.

We analyze the solutions from the point of view of their thermodynamical stability. This analysis reveals what the number L is at a given value of the applied magnetic field. On the basis of this knowledge, the *H-T* superconducting phase boundaries are calculated for the mesoscopic square loop with leads. With the definition of the *H-T* phase boundary for a square loop in terms of the ''appearance of the superconducting path,'' the obtained theoretical results agree fairly well with the experimental data.[4,5] An independent analysis performed in the framework of the London limit demonstrates that the phase boundaries are not strongly sensitive to the ''short-range'' inhomogeneities of the order parameter.

ACKNOWLEDGMENTS

This work was supported by the Interuniversitaire Attractiepolen — Belgische Staat, Diensten van de Eerste Minister — Wetenschappelijke, technische en culturele Aangelegenheden; the PHANTOMS research Network; the F.W.O.-V. project Nos. G.0287.95, G.0232.96, and the W.O.G. 0073.94N (Belgium). V.M.F. was partly supported by the Bijzonder Onderzoeksfonds (BOF) NOI 97. V.R.M. acknowledges financial support from F.W.O.-V. and the U.I.A.

APPENDIX

Substitution of the order parameter in the form of Eq. (25) into the second GL equation (2) gives

$$\Delta\mathbf{A}=-\frac{8\pi ie\hbar}{mc}\psi_a^2\nabla\phi+\frac{16\pi e^2}{mc^2}\mathbf{A}\psi_a^2. \tag{A1}$$

This allows one to represent the value of rot$\mathbf{H}$ as

$$\text{rot}\ \mathbf{H}=\text{rot}\ \ \text{rot}\ \mathbf{A}\equiv\text{grad}\ \ \text{div}\ \mathbf{A}-\Delta\mathbf{A}. \tag{A2}$$

The gauge div$\mathbf{A}=0$ implies that

$$\text{rot}\ \mathbf{H}=-\Delta\mathbf{A}, \tag{A3}$$

wherefrom, taking into account Eq. (A1), it follows that

$$\text{rot}\ \mathbf{H}=\frac{8\pi ie\hbar}{mc}\psi_a^2\nabla\phi-\frac{16\pi e^2}{mc^2}\mathbf{A}\psi_a^2. \tag{A4}$$

Integration of this identity along the *internal* boundary of the loop gives the integral relation

$$\oint_i \text{rot}\ \mathbf{H}\cdot d\,\boldsymbol{l}=\frac{8\pi ie\hbar}{mc}\oint_i\psi_a^2\nabla\phi\cdot d\,\boldsymbol{l}-\frac{16\pi e^2}{mc^2}\oint_i\psi_a^2\mathbf{A}\cdot d\,\boldsymbol{l}. \tag{A5}$$

Under the assumption that the squared amplitude of the order parameter ψ_a^2 changes along the internal boundary of the loop more slowly as compared with the gradient of the phase $\nabla\phi$ and the vector potential $\mathbf{A}$, the general integral relation (A5) can be approximately simplified to

$$\oint_i \text{rot}\ \mathbf{H}\cdot d\,\boldsymbol{l}=\frac{8\pi ie\hbar}{mc}\psi_a^2\oint_i\nabla\phi\cdot d\,\boldsymbol{l}-\frac{16\pi e^2}{mc^2}\psi_a^2\oint_i\mathbf{A}\cdot d\,\boldsymbol{l}. \tag{A6}$$

Now the contour integrals on the right-hand side are

$$\oint_i\nabla\phi\cdot d\,\boldsymbol{l}=2\pi L, \tag{A7}$$

where $L=0,1,2\ldots$ is the winding number, and

$$\oint_i\mathbf{A}\cdot d\,\boldsymbol{l}=\Phi, \tag{A8}$$

where Φ is the magnetic flux through the opening of the loop. With these definitions, Eq. (A6) takes on the final form of the integral relation (31).

*Permanent address: Department of Theoretical Physics, State University of Moldova, str. A. Mateevici, 60, MD-2009 Kishinev, Republic of Moldova.

†Permanent address: Institute of Applied Physics, str. Academiei 5, MD-2028 Kishinev, Republic of Moldova.

‡Also at Universiteit Antwerpen (RUCA), Groenenborgerlaan 171, B-2020 Antwerpen, Belgium and Technische Universiteit Eindhoven, P. O. Box 513, 5600 MB Eindhoven, The Netherlands.

[1] L. P. Lévy, G. Dolan, J. Dunsmuir, and H. Bouchiat, Phys. Rev. Lett. **64**, 2074 (1990).

[2] V. Chandrasekhar, R. A. Webb, M. J. Brady, M. B. Ketchen, W. J. Gallagher, and A. Kleinsasser, Phys. Rev. Lett. **67**, 3578 (1991).

[3] D. Mailly, C. Chapelier, and A. Benoit, Phys. Rev. Lett. **70**, 2020 (1993).

[4] V. V. Moshchalkov, L. Gielen, C. Strunk, R. Jonckheere, X. Qiu, C. Van Haesendonck, and Y. Bruynseraede, Nature (London) **373**, 319 (1995).

[5] C. Strunk, V. Bruyndoncx, V. V. Moshchalkov, C. Van Haesendonck, Y. Bruynseraede, and R. Jonckheere, Phys. Rev. B **54**, R12 701 (1996).

[6] C. Strunk, V. Bruyndoncx, C. Van Haesendonck, V. V. Moshchalkov, Y. Bruynseraede, B. Burk, C.-J. Chien, and V. Chandrasekhar, Phys. Rev. B **53**, 11 332 (1996).

[7] K. Yu. Arutyunov, V. A. Krupenin, S. V. Lotkov, A. B. Pavolotski, and L. Rinderer, Superlattices Microstruct. **21**, Suppl. A, 27 (1997).

[8] X. Zhang and J. C. Price, Phys. Rev. B **55**, 3128 (1997).

[9] M. Tinkham, Phys. Rev. **129**, 2413 (1963).

[10] C. S. Mkrtchyan and V. V. Shmidt, Zh. Eksp. Teor. Fiz. **61**, 367 (1971) [Sov. Phys. JETP **34**, 195 (1972)].

[11] Yu. N. Ovchinnikov, Zh. Eksp. Teor. Fiz. **79**, 1496 (1980) [Sov. Phys. JETP **52**, 755 (1981)].

[12] P. G. de Gennes, C. R. Seances Acad. Sci., Ser. 2 **292**, 279 (1981).

[13] A. Bezryadin and B. Pannetier, Phys. Scr. **T66**, 225 (1996).

[14] V. L. Ginzburg and L. D. Landau, Zh. Eksp. Teor. Fiz. **20**, 1064 (1950).

[15] L. D. Landau and E. M. Lifshitz, *Course of Theoretical Physics*, Vol. 9 (*Statistical Physics*, Vol. 2) (Pergamon, Oxford, 1989).

[16] P. G. de Gennes, *Superconductivity of Metals and Alloys* (Addison-Wesley, Reading, 1989).

[17] C. P. Poole, Jr., H. A. Farach, and R. J. Creswich, *Superconductivity* (Academic Press, San Diego, 1995).

[18] G. D. Smith, *Numerical Solution of Partial Differential Equations: Finite Difference Methods* (Clarendon Press, Oxford, 1978).

[19] H. J. Fink, A. López, and R. Maynard, Phys. Rev. B **26**, 5237 (1982).

[20] V. M. Fomin, V. R. Misko, J. T. Devreese, and V. V. Moshchalkov, Solid State Commun. **101**, 303 (1997).

[21] *Superconductivity*, edited by R. D. Parks (Dekker, New York, 1969).

[22] J. Berger and J. Rubinstein, Phys. Rev. Lett. **75**, 320 (1995); Physica C **288**, 105 (1997).